

Compact and efficient continuous adiabatic demagnetization refrigerator for line emission mapper

Amir E. Jahromi* and Peter J. Shirron 

NASA Goddard Space Flight Center, Cryogenics and Fluids Branch, Greenbelt, Maryland, United States

ABSTRACT. The continuous adiabatic demagnetization refrigerator (CADR) described in this paper is a compact, reliable, and highly efficient magnetic cooling system designed for the line emission mapper (LEM), a future x-ray probe mission currently being proposed. Operating at two distinct temperatures of 350 mK (T_1) and 40 mK (T_0), the CADR offers continuous cooling while efficiently rejecting heat to a cryocooler at 4 K. Shielded by ferromagnetic and high-permeability magnetic shields, the CADR minimizes interference on the focal plane assembly. With flight-proven components, the CADR provides precise temperature regulation via its sensitive and large-arrayed transition edge sensor detectors. The CADR system for LEM consists of two modular units. The high-temperature module spans from 4 K to 350 mK, comprising four stages, whereas the low-temperature module spans from 350 to 40 mK, comprising three stages. The system is designed to continuously deliver 174 μ W of useful cooling power at 350 mK and 2 μ W at 40 mK.

© The Authors. Published by SPIE under a Creative Commons Attribution 4.0 International License. Distribution or reproduction of this work in whole or in part requires full attribution of the original publication, including its DOI. [DOI: [10.1117/1.JATIS.9.4.041003](https://doi.org/10.1117/1.JATIS.9.4.041003)]

Keywords: adiabatic demagnetization refrigerator; sub-Kelvin cooling; magnetic refrigerator; cryogenic cooler; line emission mapper

Paper 23075SS received Jul. 26, 2023; revised Sep. 27, 2023; accepted Sep. 29, 2023; published Oct. 20, 2023.

1 Introduction

Line emission mapper (LEM) is a groundbreaking x-ray probe currently being proposed,¹ and it is designed to tackle the fundamental challenge of understanding galaxy formation by mapping the circumgalactic medium (CGM) and intergalactic medium (IGM). With its unique features and advanced technology, such as its large 1600 cm² collecting area x-ray mirror and a state-of-the-art cryogenic microcalorimeter detectors system, LEM represents a significant leap forward in observational capabilities within the soft x-ray band. These components enable LEM not only to detect and study the CGM and IGM but also to provide high angular resolution (18 arc sec) and high spectral resolution (1.3 eV for inner arrays and 2.5 eV for the remainder arrays) imaging and spectroscopy of these diffuse sources.

Critical to LEM's success are its highly sensitive detectors, which require sub-Kelvin cooling to detect the faint x-ray emissions from the CGM and IGM. The cryogenic microcalorimeter array, utilizing transition-edge sensor (TES) technology, operates at ultra-low temperatures, in the range of 35 to 50 mK, with a current goal of 40 mK. This level of cooling is achieved via an advanced system incorporating multistage adiabatic demagnetization refrigerators (ADR) and a cryocooler. The aforementioned subsystems and components all lie within LEM's

*Address all correspondence to Amir E. Jahromi, amir.e.jahromi@nasa.gov

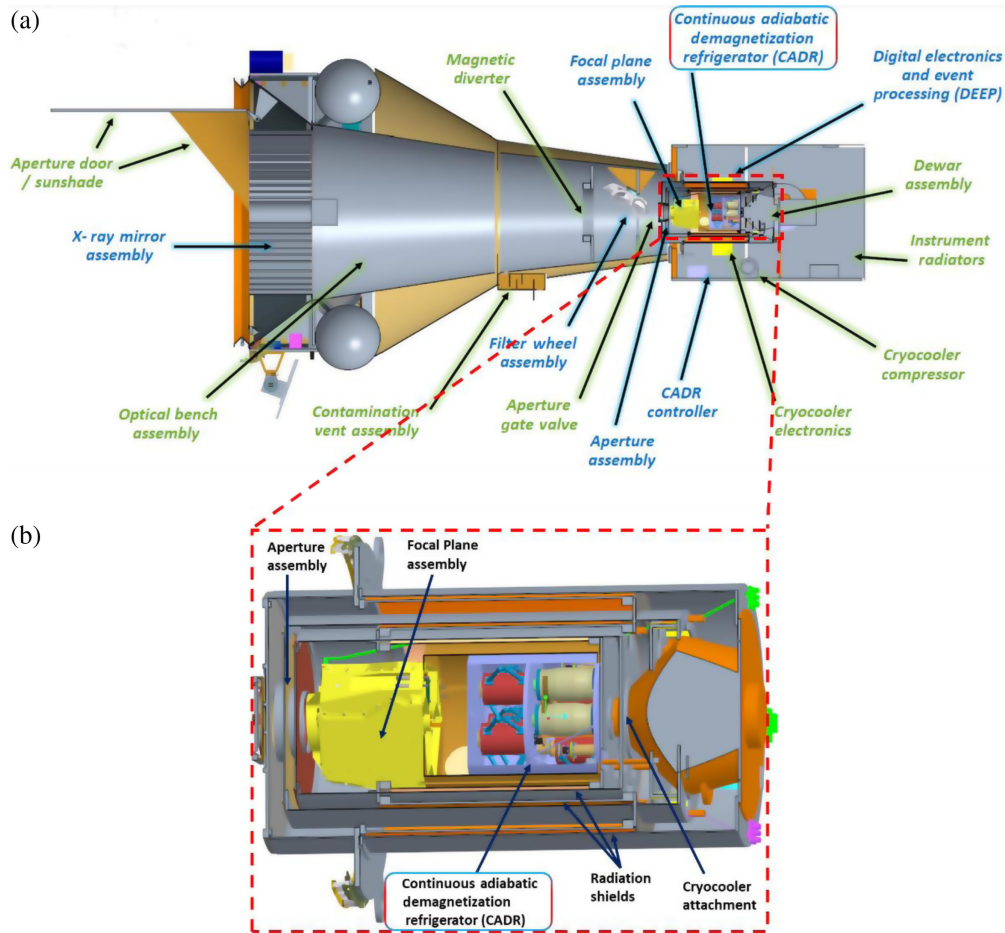


Fig. 1 (a) Cross sectional view of the LEM telescope. The CADR is shown inside the LMS, on the right side of this figure. (b) Zoomed in view of the LMS with the CADR labeled.

microcalorimeter spectrometer (LMS) compartment of the observatory. The continuous adiabatic demagnetization refrigerator (CADR)'s location is marked in Fig. 1.

The LEM detector array consists of both standard pixels with a single absorber and hydras, with the innermost absorber pixels yielding an energy resolution of 1.3 eV full-width at half-maximum (FWHM), while the remaining hydra pixels offer a resolution better than 2.5 eV (FWHM) for energies below 2 keV.² This configuration ensures accurate detection and enables the differentiation of foreground signals from our own Milky Way. These TES microcalorimeters provide outstanding energy resolution for the precise measurement of x-ray emissions thanks to its low-temperature background provided by the coldest stage of the CADR, which is responsible for continuously cooling the microcalorimeter to a very low temperature of 40 mK. In this sense, the CADR, integrated into the focal plane assembly (FPA), ensures that the microcalorimeter operates within its optimal temperature range, enabling the sensitive detection of x-ray emissions. The CADR is supported by a vacuum Dewar, featuring a single pulse-tube cryocooler that cools the core of the instrument to 4 K.³

With its unique design, cutting-edge cryogenic microcalorimeter detectors, and advanced cooling system, LEM has the potential to revolutionize our understanding of galaxy formation.² By deciphering the faint emissions of the CGM and IGM, LEM will drive breakthroughs in astrophysical research, leading to profound insights into the mysteries of the cosmos. Details related to the design of LEM's CADR are discussed in this paper.

2 CADR Requirements

In designing the CADR for LEM, the goal was to achieve a self-consistent set of hardware and operating parameters (including the input power and temperature, upper bound reject power and

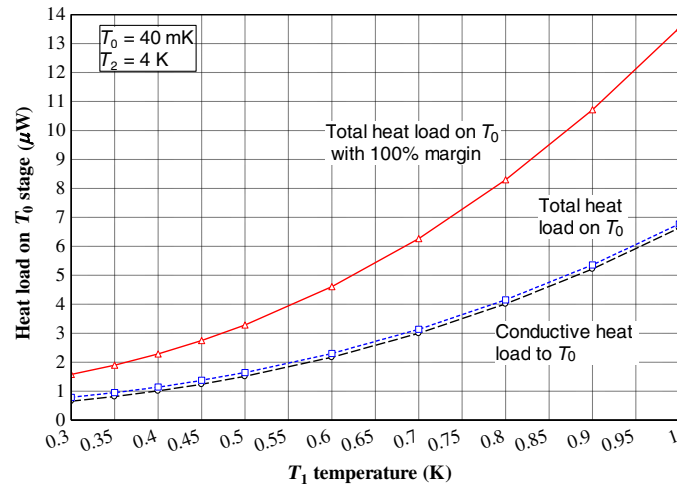


Fig. 2 Heat load contributions to T_0 as a function of T_1 temperature. Note that the external heat load on T_1 is $174 \mu\text{W}$ (including 100% margin).

temperature, cooling power, and temperature stability at each temperature node) that achieved the FPA cooling requirements within the allocation of cryocooler cooling power. The FPA houses the sensitive TES sensor arrays, anti-coincidence detectors (Anti-Co), support electronics such as superconducting quantum interference device (SQUIDs), filters, and other components. It is composed of three layers, each requiring a distinct temperature defined from coldest to warmest as T_0 , T_1 , and T_2 . The concept for LEM is similar to that for Athena's X-IFU.⁴

The T_0 subassembly is at the heart of the FPA, housing the TES detectors, Anti-Co, SQUID mux chips, and Niobium superconducting shield. This subassembly will need to be maintained at very low temperatures (40 mK) to ensure the highest sensitivity during science acquisition. This innermost structure is suspended from an intercept ring at T_1 via a Kevlar suspension. The ring accommodates heatsinking for the outer Kevlar suspension mount and the series array SQUIDs. The ring is thermally isolated from the outermost layer via a Kevlar suspension system. The outermost layer is surrounded by a high-permeability magnetic shield, accommodating heat-sinking, and transition from Dewar cables and harnesses, bias, filter, and termination banks which are all maintained at T_2 .

The CADR produces the two coldest temperatures, labeled as T_0 and T_1 . Although T_0 is 40 mK, the required cooling power is dependent on the temperatures T_1 and T_2 . The cooling for T_2 is facilitated by a cryocooler, which is sustained at a nominal temperature of 4 K. From a CADR design perspective, T_1 is a free variable that is determined by modeling a CADR that results in maximum thermodynamic efficiency while preserving the legacy of past spaceflight, balloon, and laboratory experiments to maintain an acceptable and high level of technology readiness level (TRL).⁵⁻⁷ This requires modeling the heat load on T_0 as a function of T_1 , with T_2 being fixed. The findings from this model are illustrated in Fig. 2.

The heat load from T_2 into T_1 is nearly independent from the latter temperature because conductive loads dominate and are determined almost exclusively by T_2 . The temperature stability at T_0 and T_1 is currently baselined to be $1 \mu\text{K}$ and 2 mK for any 10-min interval, respectively, which is commensurate with past demonstrations of similar ADR systems. Finally, the exported magnetic field from the CADR onto the FPA region shall be $<2 \mu\text{T}$.

Details of the CADR configuration and design are detailed in the next section.

3 CADR Architecture

The modeling of the CADR system was achieved using a simulator that was developed progressively over the past two decades for multistage ADRs and CADR, and its accuracy was most recently validated using comparisons of actual and predicted performance of the Astro-H/Hitomi and XRISM ADRs.⁸ Two major aspects needed consideration in determining the T_1 temperature within this model: (1) preserving close heritage to past systems and (2) arranging the ADR stages

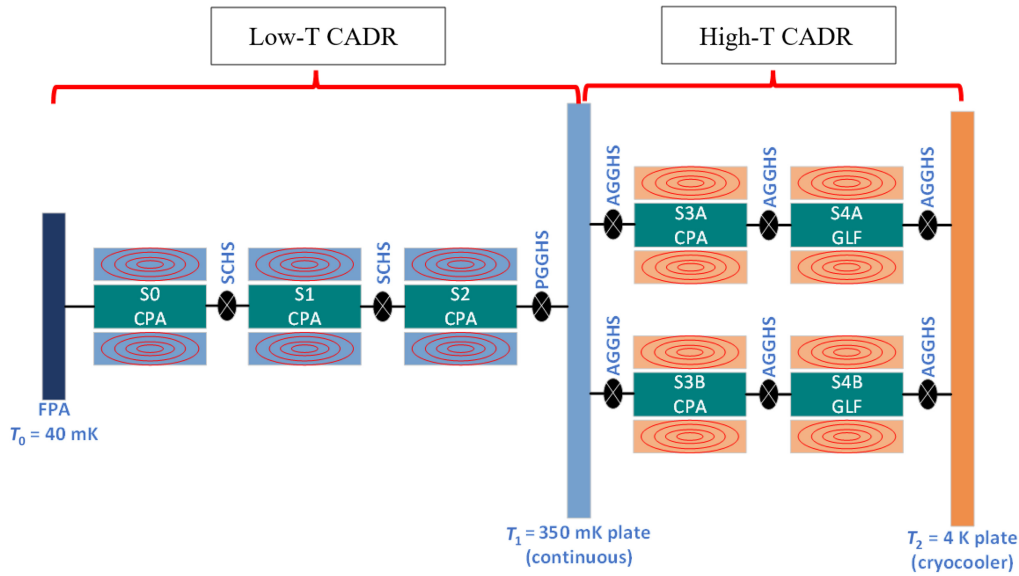


Fig. 3 Schematic of LEM's seven-stage CADR: four stages comprise the high- T CADR and three-stages comprise the low- T CADR. (AGGHS, active gas gap heat switch; PGGHS, passive gas gap heat switch; SCHS, super conducting heat switch; CPA, chromium potassium alum; and GLF, gadolinium lithium fluoride).

in a way that yields the highest thermodynamic efficiency. This approach involved reducing the T_1 temperature to 350 mK, thereby minimizing the heat load onto T_0 while ensuring high-heat throughput from T_1 to T_2 . Figure 3 provides a schematic of the resulting CADR for LEM. This model encompasses seven stages and is arranged as two operationally independent modular subsystems: the high- T CADR, consisting of four stages, and the low- T CADR, consisting of three stages. Details of each module are described in the subsequent two sections.

3.1 High- T CADR

As shown in Fig. 4, the high- T CADR is configured as two assemblies in parallel, each composed of two stages in series. The superconducting magnets for each of these stages are thermally sunk

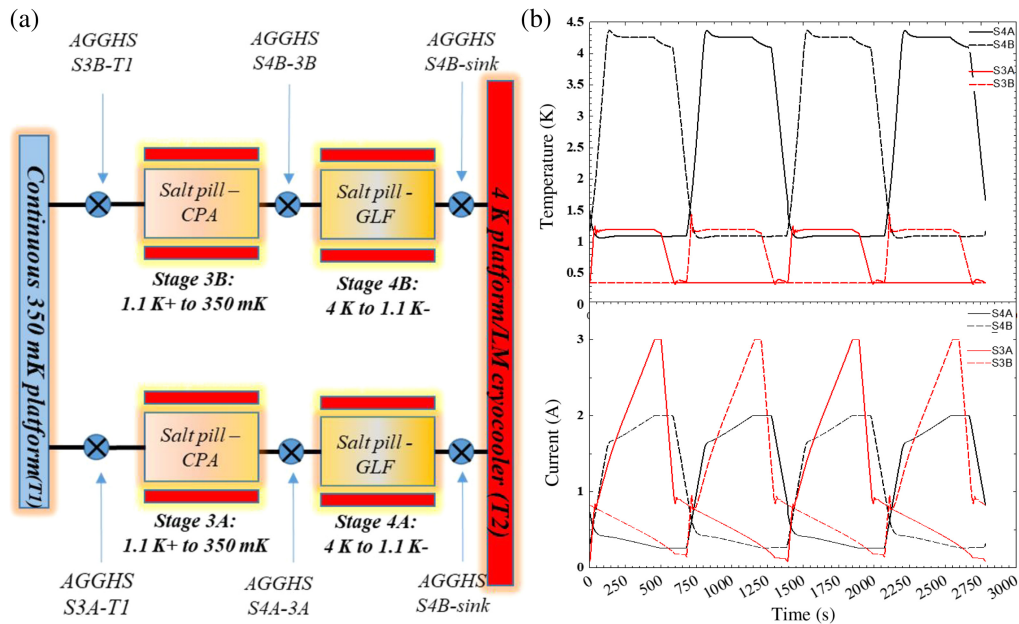


Fig. 4 (a) Schematic of the four-stage high- T CADR and (b) temperature and current profiles produced by the high-fidelity simulator shown toward the top and bottom, over two full cycles.

Table 1 Key parameters related to the high- T CADR module.

	Refrigerant (g)	Field to current ratio (T/A)	Max current (A)	Upper T (K)	Lower T (K)	Mass (kg)
Stage 4A	GLF: 150	1.5	2	4.3	1.1	4.12
Stage 4B	GLF: 150	1.5	2	4.3	1.1	4.12
Stage 3A	CPA: 100	0.38	3	1.3	0.35	2.2
Stage 3B	CPA: 100	0.38	3	1.3	0.35	2.2

at the base plate temperature of 4 K. A total of six active gas gap heat switches (AGGHS), identical to those used on Hitomi and XRISM,⁹ facilitate making and breaking the thermal connection between the stages, heat source, or heat sink at appropriate times in the cycle. Although this configuration necessitates more components and introduces additional complexity into operation, particularly during control handover between stages 3A and 3B compared with a purely serially configured counterpart, it offers two main advantages: it employs less massive stages and enables a higher heat throughput from 350 mK to 4 K. This increased heat throughput is necessary to achieve the cooling power required at 350 mK explained below within the fraction of the cryocooler's total cooling power allocated to the CADR.

The main sources of heat at 350 mK must be absorbed by either stage 3A or 3B during operation at this temperature. These are (1) the heat load from the FPA intercept ring and attachments; (2) the heat rejected by the low- T CADR, including hysteresis losses from the superconducting magnets of the three lower stages; and (3) parasitic heat from the mechanical structure that thermally isolates the high- T CADR from the low- T CADR. A detailed model of the latter heat loads, internal-to-CADR, on the 350 mK platform is estimated to be $\sim 330 \mu\text{W}$. Adding the $174 \mu\text{W}$ external-to-CADR load, the total heat load is $\sim 500 \mu\text{W}$. The high- T CADR is designed to handle this heat load at T_1 .

Each cycle of the high- T CADR will take ~ 25 min. The current and temperature profiles produced by the high-fidelity simulator are also shown in Fig. 4. The heat rejected to the cryocooler at 4 K follows a cooling curve provided by the manufacturer and is programmed to not exceed 14 mW at any time in the cycle. The CADR duty cycle during reject to the 4 K cryocooler is 70%, whereas the duty cycle for absorbing heat at 350 mK is at 100%. Some key parameters related to the high- T CADR are tabulated in Table 1.

3.2 Low- T CADR

As shown in Fig. 5, the low- T CADR is configured as three serial stages. The superconducting magnets for each of these stages are thermally sunk at the 350 mK plate. Two superconducting heat switches,⁹ between stage 0 and stage 1 and between stage 1 and stage 2, allow for making and breaking the thermal connection during appropriate times in the cycle. The required on-state conductance of these switches must be 4.4 and 22 mW/K, respectively. Stage 2 is connected to the 350 mK platform via a passive gas gap heat switch (PGGHS).¹⁰ The key design feature here is spanning the 40 to 350 mK among three stages: one stage (stage 0) is always controlled at 40 mK, and the other two stages break the temperature range into two smaller spans with the goal of ultimately reducing the parasitic heat load to its lower adjacent temperature stage while it is thermally recycling to the upper temperature stage. This key design element allows for higher efficiency in the low- T CADR chain. This serial configuration allows for precision temperature control at 40 mK, which is important for the sensitive detectors. All three stages are thermally anchored to the 350 mK platform. Thus, in addition to the power reject of this chain, each stage's superconducting magnet hysteresis loss is also dumped into the 350 mK platform.

Each cycle of the low- T CADR will take ~ 40 min. The cycle time is slowed deliberately to allow for spreading the recycled heat from stage 2 into the 350 mK platform such that it does not overwhelm the high- T CADR. (Note that there is no requirement for synchronizing the cycling of the low- T and high- T CADRs.) The current and temperature profiles produced by the high-fidelity simulator are also shown in Fig. 5. The CADR duty cycle during reject to the 350 mK platform is 80%, whereas the duty cycle for absorbing heat at 40 mK is at 100%. Some key parameters related to the low- T CADR are tabulated in Table 2.

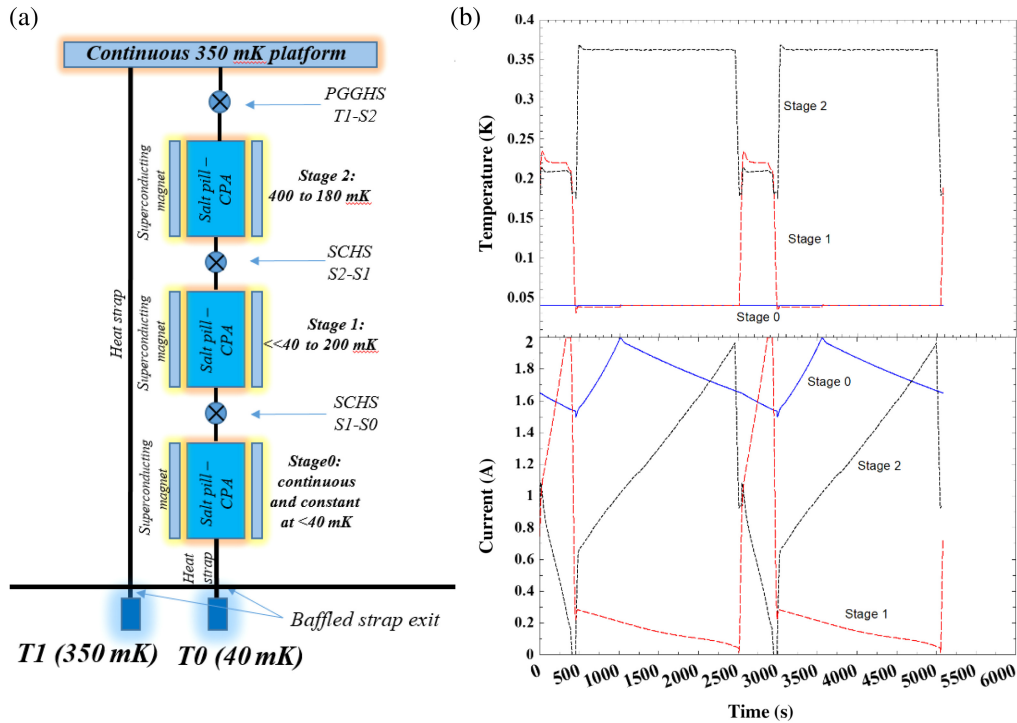


Fig. 5 (a) Schematic of the three-stage low- T CADR and (b) temperature and current profiles produced by the high-fidelity simulator shown toward the top and bottom, respectively.

Table 2 Key parameters related to the low- T CADR module.

	Refrigerant (g)	Field to current ratio (T/A)	Max current (A)	Upper T (K)	Lower T (K)	Mass (kg)
Stage 2	CPA: 100	0.2	2	0.4	0.180	2.0
Stage 1	CPA: 100	0.1	2	0.200	0.035	1.44
Stage 0	CPA: 100	0.05	2	0.04	0.04	1.44

4 CADR System Overview

In addition to the core of the CADR system already detailed, there are several other components that deserve discussion. These components include the electronics for controlling the CADR cycle, the support structure and intermediate platform at 350 mK, the overall shield, and the current leads that deliver current to each stage's superconducting magnet. In this section, they are briefly discussed, and the key overall parameters are summarized in Table 3.

The electronics responsible for controlling the CADR operation are referred to as ADR-C (ADR controller). This subsystem for LEM is baselined on past units already demonstrated with the Astro-H/Hitomi and XRISM flight ADRs.¹¹ The ADRC controls each stage independently and is therefore well-suited for both single-shot systems and CADR. It is (re-)programmable on the fly so that its control can be optimized as the performance of the system is monitored and adjustments are identified to improve cooling power and/or temperature stability. Minor modifications to the logic will be necessary, and the maximum current compatibility will need to be adjusted from 2 to 3 A to ensure full compatibility of the ADR-C with LEM's CADR.

The 350 mK platform must fulfill multiple requirements, including meeting thermal specifications, accommodating the mass of the low- T CADR stages, and being supported by the main 4 K plate that houses the high- T CADR stages. To achieve this, a hexapod structure made of carbon composite material (T-300) is employed. The hexapod structure is carefully designed to minimize parasitic heat loads from 4 K to 350 mK while ensuring structural integrity to withstand the rigorous vibrational loads experienced during launch. Figure 6 depicts a computer-aided

Table 3 Key CADR system parameters.

<i>Low-T CADR</i>	
T_0 temperature	40 mK
T_0 stability (rms)	1 μ K
Cooling power at T_0 (w/100% margin)	2 μ W
Cooling duty cycle	100%
<i>High- T CADR</i>	
T_1 temperature	350 mK
T_1 stability (rms)	2 mK
Useful cooling power at T_1 (w/ 100% margin)	174 + μ W
Cooling duty cycle	100%
T_2	
T_2 temperature	4.0 K
Peak CADR reject power	14 mW (margin accounted for at inputs)
Peak CADR reject duty cycle	70%
<i>Overall</i>	
Magnetic flux density exported at FPA	2 μ T
Exported vibration	None
First mode resonant frequency of system	>150 Hz
Total mass of system	23.9 kg

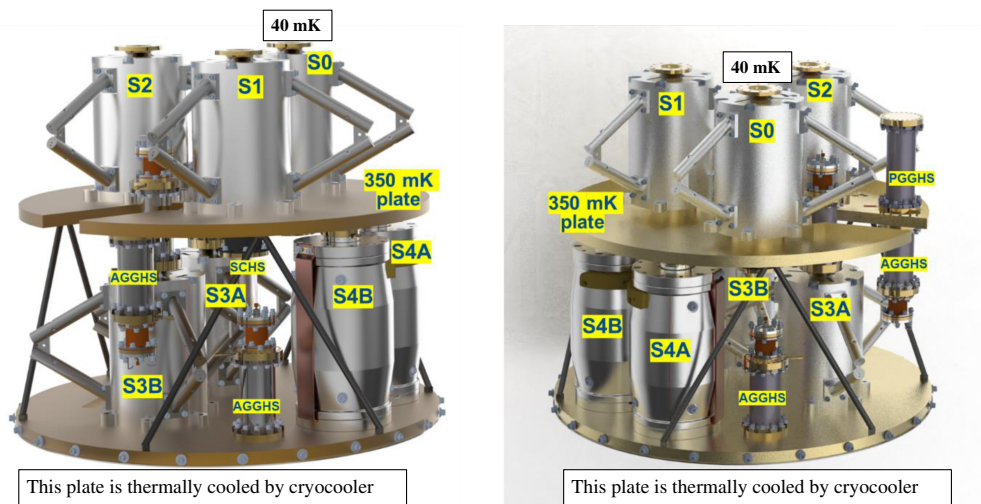


Fig. 6 CAD rendered view of LEM's CADR with the intermediate temperature platform at 350 mK and the hexapod support at two different azimuthal angles. Each stage consists of a paramagnetic salt suspended either via Kevlar or Vespel inside a superconducting magnet and surrounded by a ferromagnetic shield.

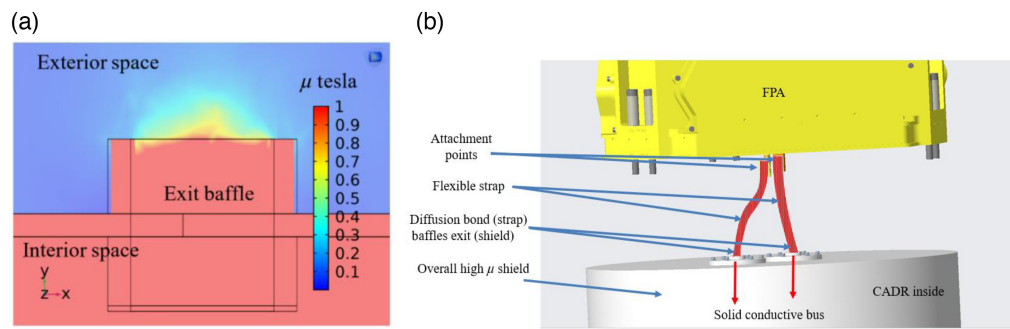


Fig. 7 (a) Analysis result of the exit baffle showing the proper level of shielding. (b) CAD model overlaid with the thermal strap concept between CADR and FPA.

design (CAD) rendered view of the CADR system, featuring the 350 mK platform and hexapod structure.

The CADR system will be enclosed within a high permeability magnetic shield to ensure that the magnetic field emitted by the stages remains below the $2 \mu\text{T}$ limit specified by the LMS requirements. This shielding is in addition to each stage's ferromagnetic shield. To allow the thermal straps to exit the shield without compromising the field requirement, carefully designed exit baffles will be implemented. These exit baffles will enable highly conductive thermal straps to pass through while maintaining the integrity of the shield. The thermal straps themselves need to be compliant and flexible, and as they emerge from the shield baffles, they will transition from solid bus structures to thin, multifoiled straps. This transition is necessary to prevent the transmission of minute vibrations originating from the cryocooler, which could introduce unwanted microphonics to the sensitive detectors. Figure 7 illustrates the concept of these thermal straps.

Finally, high-temperature superconductor (HTS) leads will deliver the current required for each stage's superconducting magnet similar in implementation to Hitomi.¹² The purpose of the HTS is to provide thermal isolation from the higher temperature stage of the cryocooler (e.g., 50 K) to the 4 K stage. This concept has flight heritage through prior flight missions.

The key CADR system parameters are summarized in Table 3.

5 Conclusion

The CADR described in this paper introduces a sophisticated architecture consisting of a low- T CADR and a high- T CADR. The high- T CADR comprises a four-stage high-temperature module and the low- T CADR comprises a three-stage low-temperature module, each designed to meet specific cooling requirements.

The high- T CADR operates at 350 mK. The parallel arrangement of stages is driven by the need for high heat throughput from 350 mK to 4 K to meet the cooling power requirement. The module incorporates AGGHSs for precise control of thermal connections between stages and allowing for priming of the system and gradual cooling from a base 4 K.

The low- T CADR operates at 40 mK and consists of three serially configured stages. This arrangement enables precision temperature control that is crucial for the sensitivity of the detectors and minimize the time-average heat load to the 40 mK stage. The module utilizes superconducting heat switches and a PGGHS to facilitate thermal connections and optimize heat recycling between stages.

The CADR's integration within the LEM mission showcases its advanced cooling capabilities, precise temperature regulation, and compatibility with flight-proven components. This breakthrough technology enables transformative measurements and observations in x-ray astrophysics, paving the way for new discoveries and enhancing our understanding of the universe.

Code, Data, and Materials Availability

The manuscript does not contain information that requires sharing code, data, etc. Additionally, the program used to generate the only simulation results plot in the manuscript cannot be shared due to proprietary reasons (per NASA).

References

1. R. Kraft et al., “Line emission mapper probing physics of cosmic ecosystems,” *Astrophys. Instrum. Methods Astrophys.* (2022).
2. S. Bandler et al., “The line emission mapper microcalorimeter spectrometer,” *J. Astron. Telesc. Instrum. Syst.* **9**(4), 041002 (2023).
3. E. Osborne et al., “Line emission mapper cryogenic system design,” *J. Astron. Telesc. Instrum. Syst.* **9**(4), 041007 (2023).
4. H. J. Van Weers et al., “The X-IFU focal plane assembly design progress and development model feedback,” *Proc. SPIE* **12181**, 121810N (2022).
5. P. Shirron et al., “A compact, high-performance continuous magnetic refrigerator for space missions,” *Cryogenics* **41**(11–12), 789–795 (2001).
6. M. O. Kimball et al., “Piper continuous adiabatic demagnetization refrigerator,” Space Cryogenics Workshop. No. GSFC-E-DAA-TN43944 (2017).
7. P. J. Shirron et al., “Design and on-orbit operation of the soft x-ray spectrometer adiabatic demagnetization refrigerator on the Hitomi observatory,” *J. Astron. Telesc. Instrum. Syst.* **4**(2), 021403 (2018).
8. P. J. Shirron et al., “Design of a 3-stage ADR for the soft X-ray spectrometer instrument on the Astro-H mission,” *Proc. SPIE* **7732**, 773212 (2010).
9. M. J. DiPirro and P. J. Shirron, “Heat switches for ADRs,” *Cryogenics* **62**, 172–176 (2014).
10. M. O. Kimball et al., “Passive gas-gap heat switches for use in low-temperature cryogenic systems,” in *IOP Conf. Ser. Mater. Sci. and Eng.*, IOP Publishing, Vol. **278** (2017).
11. M. Tsujimoto et al., “In-orbit operation of the ASTRO-H SXS,” *Proc. SPIE* **9905**, 99050Y (2016).
12. E. R. Canavan et al., “The Astro-H high temperature superconductor lead assemblies,” *Cryogenics* **64**, 194–200 (2014).

Amir E. Jahromi has been a NASA cryogenic engineer since 2012 and has made vital contributions to R&D, space missions, and balloon projects at Goddard Space Flight Center’s Cryogenics and Fluids Branch. Currently, he leads a ROSES-SAT project for a high TRL ultra-low-temperature continuous ADR. Prior to NASA, he pioneered a superfluid magnetic pump and a sub-Kelvin active magnetic regenerative refrigeration system in his dissertation, earning his PhD from the University of Wisconsin–Madison. He also developed a dry Joule-Thomson 1 K facility during his master’s studies.

Peter J. Shirron is a renowned cryogenic engineer with three decades of experience at NASA’s Goddard Space Flight Center and earned his PhD in low-temperature physics in 1989. He served as an editor of the *Cryogenics Journal* at Elsevier Publishing from 2014 to 2022 and was president of the Cryogenic Society of America from 2018 to 2020. He has made significant contributions to many R&D, spaceflight, and balloon missions at NASA’s Goddard Space Flight Center and holds multiple patents. He is the inventor of the continuous cycle ADR.